


Article

Performance Assessment of SWRO Spiral-Wound Membrane Modules with Different Feed Spacer Dimensions

A. Ruiz-García ^{1,*}  and I. Nuez ²

¹ Department of Mechanical Engineering, University of Las Palmas de Gran Canaria, 35017 Las Palmas de Gran Canaria, Gran Canaria, Spain

² Department of Electronic and Automatic Engineering, University of Las Palmas de Gran Canaria, 35017 Las Palmas de Gran Canaria, Gran Canaria, Spain; ignacio.nuez@ulpgc.es

* Correspondence: alejandro.ruiz@ulpgc.es; Tel.: +34-928-451-888

Received: 18 May 2020; Accepted: 11 June 2020; Published: 14 June 2020



Abstract: Reverse osmosis is the leading process in seawater desalination. However, it is still an energy intensive technology. Feed spacer geometry design is a key factor in reverse osmosis spiral wound membrane module performance. Correlations obtained from experimental work and computational fluid dynamics modeling were used in a computational tool to simulate the impact of different feed spacer geometries in seawater reverse osmosis spiral wound membrane modules with different permeability coefficients in pressure vessels with 6, 7 and 8 elements. The aim of this work was to carry out a comparative analysis of the effect of different feed spacer geometries in combination with the water and solute permeability coefficients on seawater reverse osmosis spiral wound membrane modules performance. The results showed a higher impact of feed spacer geometries in the membrane with the highest production (highest water permeability coefficient). It was also found that the impact of feed spacer geometry increased with the number of spiral wound membrane modules in series in the pressure vessel. Installation of different feed spacer geometries in reverse osmosis membranes depending on the operating conditions could improve the performance of seawater reverse osmosis systems in terms of energy consumption and permeate quality.

Keywords: desalination; reverse osmosis; feed spacers; seawater; membrane performance; permeability coefficients

1. Introduction

Seawater desalination has become one of the main solutions to the worldwide problem of water scarcity. Among the available technologies, reverse osmosis (RO) is widely regarded as being the most efficient and reliable [1]. However, seawater RO (SWRO) is an intensive energy consumption process [2,3]. Optimizing the design and operation of SWRO desalination plants is one of the various ways to reduce the specific energy consumption (SEC) [4–6]. A key factor in this respect is the SWRO membrane technology that is used [7,8]. In spiral-wound membrane modules (SWMMs), the permeability coefficients have a significant impact on plant performance in terms of production and solute rejection [9,10]. Important efforts are being made to try to inhibit the effect of fouling on the permeability coefficients during plant operation by improving the pretreatment process [11] and increasing the resistance to fouling [12]. Another important characteristic of SWRO SWMMs is the feed spacer geometry (FSG) [13,14]. The FSG plays an important role in the concentration polarization (CP) phenomena and the pressure drop along the SWMMs [15–17].

In the optimal design and operation of SWRO systems, consideration of the water and solute permeability coefficients (A and B , respectively) in conjunction with the FSG is fundamental.

Different optimal FSGs and different operation windows have been obtained for different A and B [14]. Several works have shown the impact of FSGs on the hydrodynamics in the feed channel of SWMMs, which affect other parameters. G. Schock and A. Miquel [18] obtained correlations for the friction factor (λ) and the Sherwood number (Sh) for RO membranes in a spiral-wound configuration through experimental work. λ depends on the Reynolds number (Re) and on two correlative parameters, and Sh depends on Re , the Schmidt number (Sc) and three correlative parameters. Sh is associated to the mass transfer coefficient (k) and therefore to the polarization factor (PF). V. Geraldès et al. [19] changed the equation obtained for λ by including other parameter (K_λ) in order to consider pressure gradients in the inlet of the pressure vessels (PVs) and SWMM fittings. This equation was used to simulate and optimize a medium-sized SWRO system. A. Abbas [20] used a different correlation for λ but analogous to the previous one. This correlation was obtained in an earlier work [21] and for different membranes (ultrafiltration). The mentioned correlation require the use of Re and three correlative parameters. It was used for the simulation of an industrial water desalination plant. In 2004, J. Schwinge et al. [22] used the equation obtained in a previous work [21] but a parameter was removed from the correlation. The aforementioned studies investigated the fouling effect in SWMMs by using computational fluid dynamics (CFD). These former works did not allow the use of diverse FSGs, which have different parameters (λ and Sh respectively) for the calculation of pressure drop and PF . C.P. Koutsou et al. [23] improved the previous works by putting forward different equations for the calculation of dimensionless pressure drop (proportional to λ), taking into consideration geometric characteristics of the feed spacers such as the ratio of the distance between parallel filaments and the filament diameter (L/d), the angle between the crossing filaments (β) and the flow attack angle (α). In a subsequent work, C.P. Koutsou et al. [24] used the equation obtained by G. Schock and A. Miquel to calculate the Sh for different FSGs. One of the main advantages of the correlations obtained by C.P. Koutsou et al. [24] is the applicability in full-scale RO systems due to the short computation time required for calculation, contrary to CFD. Usually, CFD studies are focused on the design of the FSGs itself rather than in their impact of existing FSGs on full-scale RO desalination plants [25–28]. A performance study of a RO process considering the pressure drop, CP phenomena and the shape of the filament was carried out by G. Guillen and E.M.V. Hoek [29]. The research was done by proposing a three-parameter correlation for λ and the usual correlation for Sh . The mentioned authors did not consider different FSGs. A.H. Haidari et al. [13] assessed the performance of six commercial feed spacers focusing on pressure drop. The impact of the CP and RO membrane characteristics were not taken into consideration in that study. Other interesting work was carried out by the same research group [30], in this work, the effect of feed spacer orientation on hydraulic conditions was studied. Assessment of pressure drop results considering different attack angles was done, higher pressure losses were observed with flow attack angle of 45° than 90° . The authors used a correlation similar to the proposed by G. Schock and A. Miquel [18] to determine λ .

Numerous studies have been published on the optimal design of RO systems. Yan-Yue Lu et al. [31] developed an optimization method for designing RO systems considering different feed concentrations and permeate specifications. The algorithm used by these authors allowed the integration of different SWMMs in the PV. The equations used for pressure losses and the mass transfer coefficient (k) were the same as used by A. Abbas [20]. A multi-objective optimization algorithm was developed by F. Vince et al. [32]. The method optimized the SEC and permeate flux in relation to the cost of the permeate. Pressure losses were calculated by using an equation proposed by the membrane manufacturer. K.M. Sassi and I.M. Mujtaba [33] proposed optimization of the operation of an RO desalination process which used SWMMs by considering membrane fouling. The SEC was optimized at a fixed permeate flow rate and quality. The correlation proposed by A.R. Dacosta [21] was used to estimate pressure losses and k . Y. Du et al. [34] proposed an optimization method considering both SWRO and brackish water RO desalination systems with SWMMs. They considered the correlation proposed by V. Geraldès et al. [19] for pressure loss estimation and the correlation proposed by A.R. Dacosta [21] for k estimation. A. Altaee [35] developed a computational model for

the design and performance estimation of SWRO systems. Equations proposed by the membrane manufacturer for pressure losses and PF were used in that work. The same equations were used by E. Ruiz-Saavedra et al. [36,37] in their development of a design method for brackish water RO systems. June-Seok Choi et al. [38] centered their work around the optimization of two-stage SWRO systems. Equations obtained in another published work [39] for pressure losses and k were used. A computational tool for designing brackish water RO systems with SWMMs was developed by A. Ruiz-García and I. Nuez [40]. This tool allowed the use of different FSGs, but simulations using different FSGs in brackish water RO SWMMs were not provided.

To evaluate the impact of the different FSGs in a full-scale PV with commercial SWRO SWMMs requires simple equations that can be used without the high computational requirements of CFD modeling. This is the main motive to use simple correlations such as those proposed by some mentioned authors [18,23,24] are needed. Another important matter that should be considered concerns the membrane permeability coefficients A and B . The values of A and B are key in the optimization of the performance of SWMMs considering different FSGs. In full-scale SWRO desalination plants, slight variations SEC could have large repercussions on operation and maintenance costs. This paper aims to simulate a PV with full-scale SWRO SWMMs under a range of feed flow (Q_f), feed pressure (p_f) and feed concentration (C_f) characteristics, considering different membrane permeability coefficients (A and B) and FSGs.

The following sections are the methodology where characteristics of the selected SWMMs, process modeling and calculation algorithm are described; results and discussion where the performance analysis of the considered PVs that contain SWMMs with different FSGs is presented; and finally the conclusions of this work including future research lines that should be taken into consideration from now on.

2. Methodology

Two SWRO SWMMs were considered, FILMTEC™ SW30XLE-400 and FILMTEC™ SW30XHR-400 from Dupont®, Wilmington, Delaware, USA. The Water Application Value Engine (WAVE) software from Dupont® company was employed to determine the coefficients A and B of the SWMMs under test conditions. Table 1 shows the calculated coefficients A and B . These SWRO membranes were selected due to their different characteristics (high production (SW30XLE-400) and high rejection (SW30XHR-400)). The mentioned characteristics are key in the operation of full-scale SWRO desalination plants. Both characteristics are related, through the membrane permeability coefficients A and B , with the performance of the desalination process in terms of SEC and permeate quality.

Table 1. SWRO membrane permeability coefficients under test conditions.

SWMM	A_0 (m Pa ⁻¹ s ⁻¹)	B (m s ⁻¹)
FILMTEC™ SW30XLE-400	3.71×10^{-12}	1.93×10^{-8}
FILMTEC™ SW30XHR-400	2.47×10^{-11}	1.16×10^{-8}

To carry out a comparative study of the two full scale SWRO membranes, PVs of 6–8 elements were simulated. A C_f range of between 32 and 45 kg m⁻³ of sodium chloride (NaCl) was used with feed flow (Q_f) and feed pressure (p_f) ranges from 3 to 16 m³ h⁻¹ and from 40 to 80 bar, respectively. The different FSGs studied by C.P. Koutsou et al. [23] were used. The solution-diffusion transport model [41–43], which presumes that the RO membrane does not have porous or imperfections, was utilized. This model is based on considering that each solvent and solute are dissolved in the membrane separately on the feed-brine side and then diffused in individual fluxes through the membrane under the effect of pressure and concentration gradients (Equations (1) and (2)). This is the most extended model and provides results close to the real behavior of RO systems for both seawater and brackish water [44]. The transport equations used the mean values of each SWRO

SWMM, and pressure gradients in the permeate carrier as well as temperature changes along the SWRO SWMMs were disregarded. The solvent (permeate) flow is described by Equation (1) and the solute flow by Equation (2).

$$Q_p = A \cdot (\Delta p - \Delta \pi) \cdot S_m \quad (1)$$

where Q_p is the permeate flow, Δp is the pressure gradient across the membrane, $\Delta \pi$ is the osmotic pressure gradient across the membrane and S_m is the active membrane surface.

$$Q_s = B \cdot \Delta C \cdot S_m \quad (2)$$

where Q_s is the solute flow across the membrane, and ΔC is the concentration gradient of solute on either side of the membrane.

Coefficient A (Equation (1)) was considered to depend on two variables (Equation (3)): feed temperature (T) and flow factor (related to fouling and operating time (FF)) [40]. The effect of the CP on coefficient A was not considered. As the RO SWMMs get fouled the Q_p decreases under a fixed p_f which means that the coefficient A decreases. FF is an important parameter that affects the coefficient A due to fouling [45]. Various methods have been proposed to try to predict the value of this parameter [46]. This work regards a comparative study between using different FSGs in two different SWRO SWMMs. It was considered that the flow factor FF was 1 (membrane without fouling). Usually, the FF decreases with operating time as the SWMMs get fouled [45]. A T of 25 °C was considered, so the temperature correction factor (TCF) had a value of 1.

$$A = A_0 \cdot TCF \cdot FF \quad (3)$$

where A_0 is the initial value of A . The net driving pressure (NDP) depends on p_f , pressure drop (Δp_{fb}), permeate pressure (p_p), average osmotic pressure on the membrane surface (π_m) and average osmotic pressure of the permeate (π_p):

$$NDP = (\Delta p - \Delta \pi) = p_f - \frac{\Delta p_{fb}}{2} - p_p - \pi_m + \pi_p \quad (4)$$

Δp_{fb} was calculated as follows [40,47]:

$$\Delta p_{fb} = \lambda \cdot L \cdot \frac{\rho_{fb}}{d_h} \cdot \frac{v_{fb}}{2} \quad (5)$$

$$d_h = \frac{4\varepsilon}{\frac{2}{h} + (1 - \varepsilon)\frac{8}{h}} \quad (6)$$

$$\rho_{fb} = 498.4 \cdot M + \sqrt{248,400 + 752.4 \cdot C_{fb} \cdot M} \quad (7)$$

where

$$M = 1.0069 - 2.757 \times 10^{-4} \cdot T \quad (8)$$

where L is the SWMM length (taken as 1 m), ρ_{fb} is the average feed-brine density (kg m^{-3}), M is an empirical parameter, v_{fb} is the average feed-brine water velocity (m s^{-1}), d_h (m) is the hydraulic diameter of the feed channel, ε is the porosity of the cross-sectional area of the feed channel (assumed 0.89 [18]) and h is the height of the feed channel, which was taken as 7.11×10^{-4} m (28 milli-inches) for the two SWMMs. In this study, pressure losses in the permeate channel were not considered, and a value of $p_p = 34,473.8$ Pa (5 psi) was considered [48]. Figure 1 shows the different FSG parameters. The correlations used for λ were those proposed by C.P. Koutsou et al. [23] (Table 2). λ was multiplied by the parameter K_λ , which was introduced by V. Geraldès et al. [19]. Values between 1.9 and 2.9 were obtained in that study.

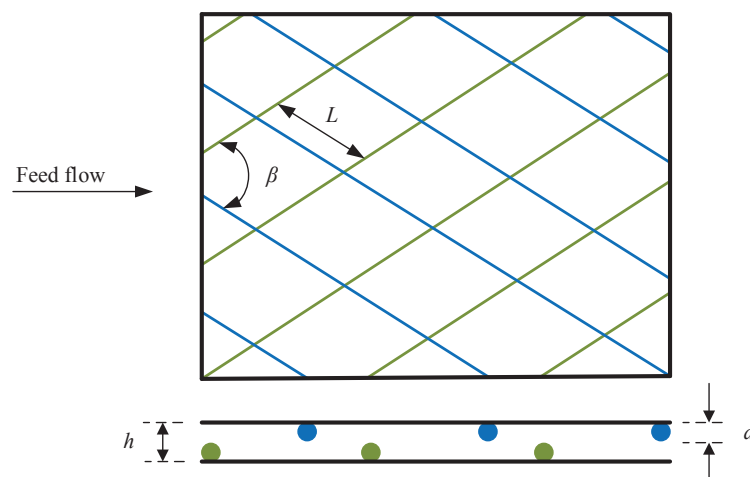


Figure 1. Parameters of FSGs [14].

Table 2. Correlation for λ calculation considering different FSGs [23].

	$\beta = 90^\circ$	$\beta = 105^\circ$	$\beta = 120^\circ$
$L/d = 6$	$2.3Re^{-0.31}$	$2.2Re^{-0.23}$	$3.8Re^{-0.18}$
$L/d = 8$	$0.8Re^{-0.19}$	$0.9Re^{-0.15}$	$1.2Re^{-0.14}$
$L/d = 12$	$1.5Re^{-0.40}$	$1.1Re^{-0.31}$	$0.7Re^{-0.19}$

Due to CP phenomena, the solute concentration on membrane surface increases. This concentration generates a diffusive reverse flow to the feed-brine bulk. Once steady state conditions are established, the PF provides the relationship between the average concentration of solute on the membrane surface (C_m) and the average feed-brine solute concentration (C_{fb}). Equation (12) was used to calculate π_p . This enables calculation of the solute concentration of the permeate (C_p) through Equation (9) [48]:

$$C_p = B \cdot PF \cdot TCF \cdot \frac{S_m}{Q_p} \cdot \left(\frac{C_f \cdot (1 + CF)}{2} \right) \quad (9)$$

$$\pi_m = \pi_f \cdot \frac{C_{fb}}{C_f} \cdot PF \quad (10)$$

$$CF = \frac{1}{1 - Y} \quad (11)$$

where CF is the concentration factor, π_f is the feedwater osmotic pressure and Y the fraction recovery of the SWMM. Equations (13) and (14) were obtained by using the film boundary model for CP [49].

$$\pi_f = 4.54047 \cdot \left(10^3 \cdot C_f / (M_s \cdot \rho) \right)^{0.987} \quad (12)$$

$$C_m = C_{fb} \cdot PF \quad (13)$$

$$PF = \frac{C_m}{C_{fb}} = e^{\frac{J_p}{k}} \quad (14)$$

where M_s is the molecular weight of NaCl, J_p is the permeate flow per unit of S_m and k is the mass transfer coefficient, which is obtained by Equation (15) [18]:

$$Sh = a \cdot Re^b \cdot Sc^c = \frac{k \cdot d_h}{D} \quad (15)$$

$$Re = \frac{\rho_{fb} \cdot v_{fb} \cdot d_h}{\eta} \quad (16)$$

$$Sc = \frac{\eta}{\rho_{fb} \cdot D_s} \quad (17)$$

where a , b and c are parameters, Sc is the Schmidt number, v_{fb} is the feed-brine velocity (m s^{-1}) and η ($0.000891 \text{ kg m}^{-1} \text{ s}^{-1}$ when $T = 25^\circ \text{C}$) the dynamic viscosity of pure water. C. P. Koutsou et al. [24] calculated correlations for the Sh for different FSGs (Table 3). Solute diffusivity (D_s ($\text{m}^2 \text{ s}^{-1}$)) was calculated using the Equation (18) [50]:

$$D_s = (0.72598 + 0.023087T + 0.00027657T^2) \times 10^{-9} \quad (18)$$

Table 3. Correlation for Sh calculation considering different FSGs [24].

	$\beta = 90^\circ$	$\beta = 105^\circ$	$\beta = 120^\circ$
$L/d = 6$	$0.14Re^{0.64}Sc^{0.42}$	$0.08Re^{0.715}Sc^{0.48}$	$0.073Re^{0.87}Sc^{0.45}$
$L/d = 8$	$0.16Re^{0.605}Sc^{0.42}$	$0.17Re^{0.625}Sc^{0.42}$	$0.12Re^{0.71}Sc^{0.43}$
$L/d = 12$	$0.26Re^{0.57}Sc^{0.37}$	$0.17Re^{0.64}Sc^{0.40}$	$0.19Re^{0.645}Sc^{0.38}$

In order to calculate all the above variables, an algorithm previously proposed by the authors [40] was used and implemented in MATLAB[®]. The SEC was determined by dividing the energy consumed by the high pressure pump (which was assumed to have 100% efficiency) by the permeate flow. Steps of $0.25 \text{ m}^3 \text{ h}^{-1}$, 0.5 bar and 1 kg m^{-3} were used for Q_f , p_f and C_f , respectively. If some result exceeded the constraints established by the membrane manufacturer (minimum concentrate flow of $3 \text{ m}^3 \text{ h}^{-1}$, 15% maximum element recovery), it was removed.

3. Results and Discussions

Figure 2 shows the flux recovery (R), SEC and C_p of the FILMTEC[™] SW30XLE-400 and FILMTEC[™] SW30XHR-400 SWMMs installed in a PV with 7 elements, with a $C_f = 32 \text{ kg m}^{-3}$, $L/d = 6$ and $\beta = 90^\circ$. The SW30XLE-400 has a higher coefficient A than the SW30XHR-400 (Table 1). Consequently, higher R values are reached with lower p_f than with the SW30XHR-400, but the operating window (possible operating points according with the membrane manufacturer constraints) is wider for the SW30XHR-400 than the SW30XLE-400 (Figure 2a,b). This is due to the high permeate production attained by the SW30XLE-400 membrane. As the pressure rises the concentrate flow decreases considerably, reaching the minimum established by the manufacturer with not very high pressures. This factor should be taken into account when this type of membrane is placed in PVs of 7 and 8 elements. Figure 2c,d show that low SEC values were reached with Q_f values ranging between 5 and $10 \text{ m}^3 \text{ h}^{-1}$ for both membranes. The more elements arranged in series the higher the R and the lower the SEC up to the point allowed by the minimum reject flow restriction imposed by the membrane manufacturer. The C_p decreased with increasing Q_f and p_f (Figure 2e,f) caused by coefficient B was constant, and the higher the v_{fb} the lower the PF and C_m . It should be remarked that changes in C_f and/or of the coefficients A and B (caused by fouling) could considerably vary the operating points values.

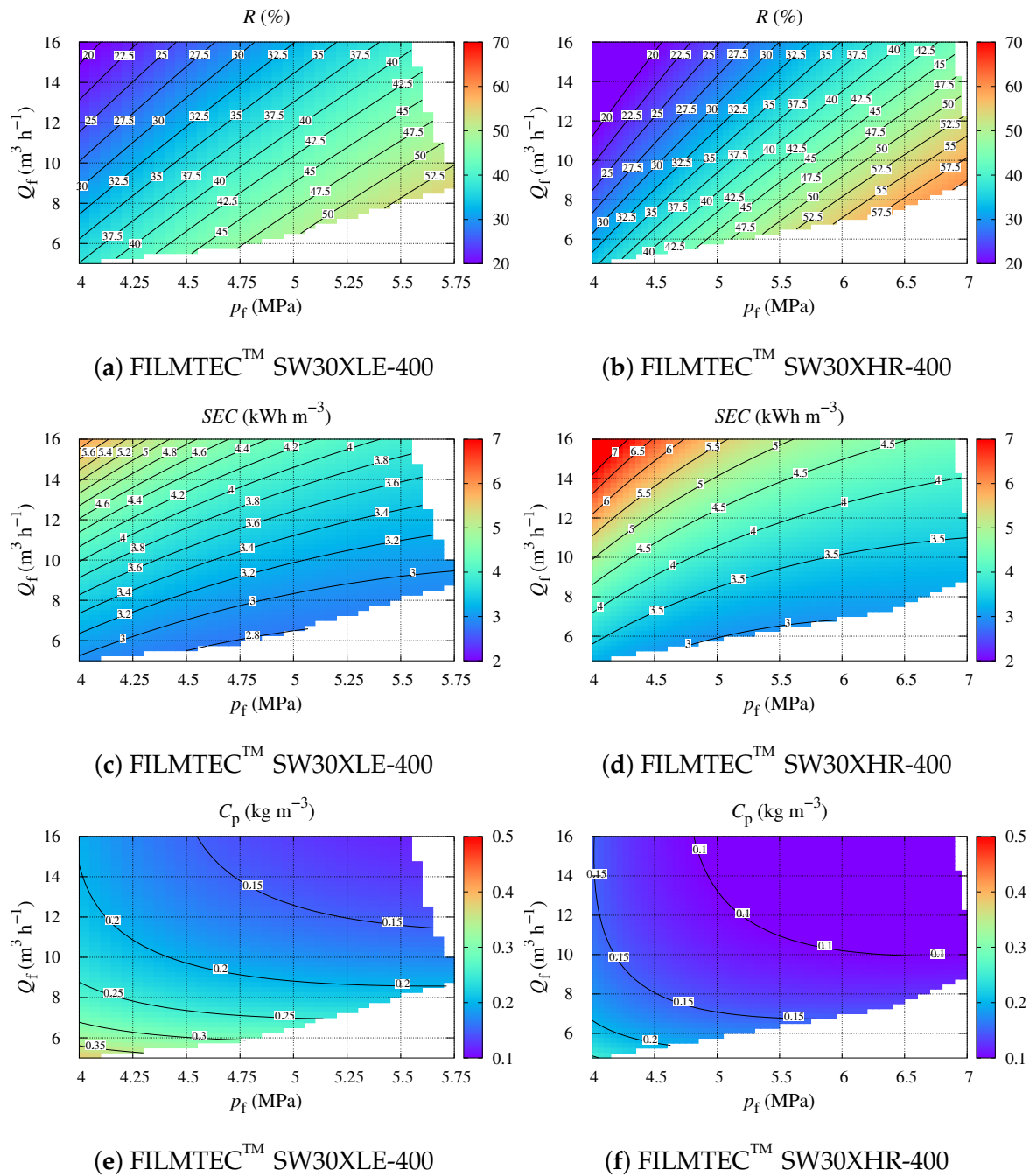


Figure 2. R , SEC and C_p of the two studied membranes with different permeability coefficients, PV with 7 SWMMs, $C_f = 32 \text{ kg m}^{-3}$, $L/d = 6$ and $\beta = 90^\circ$.

Figure 3a,b show the exponential growth of SEC with the increase of C_f . With the increment of C_f there was a small increase in the distance of the exponential curves of each FSG. The membrane with the higher coefficient A showed to have a lower SEC . Although, the separation between curves was more pronounced for the SW30XLE-400 than the SW30XHR-400 membrane. This showed that the influence of FSG with the C_f was higher for the SW30XHR-400 membrane. This was due to mentioned SWMM allowed to pass less salt (higher C_{fb}) and spite of having lower coefficient A (which make C_{fb} to decrease), the impact of having lower coefficient B was higher than having a higher A on SEC .

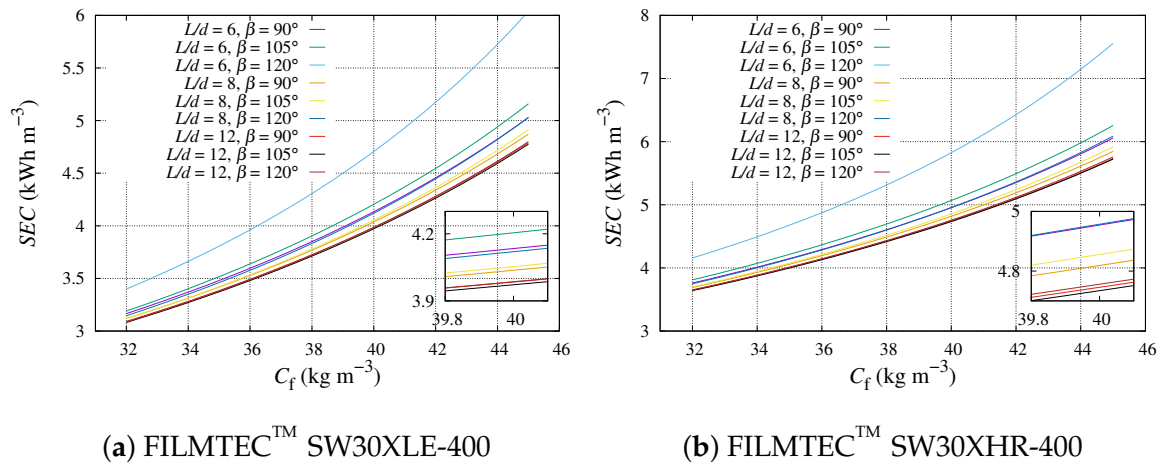


Figure 3. SEC of a PV with 8 SWMMs in series considering different FSGs, a range of C_f , $p_f = 55$ bar and $Q_f = 12 \text{ m}^3 \text{ h}^{-1}$.

As happened with SEC, C_p also showed an exponential growth with the increase of C_f for both membranes (Figure 4a,b). Again, slightly bigger differences between curves were reached at higher C_f values and were even more pronounced for the membrane with the higher coefficient A (SW30XLE-400). The C_p in the SW30XHR-400 was in a shorter range (0.1–0.25 kg m^{-3}) than in the SW30XLE-400 (0.16–0.35 kg m^{-3}). The response of the membrane with the lower B showed a more stable salt rejection for a range of C_f .

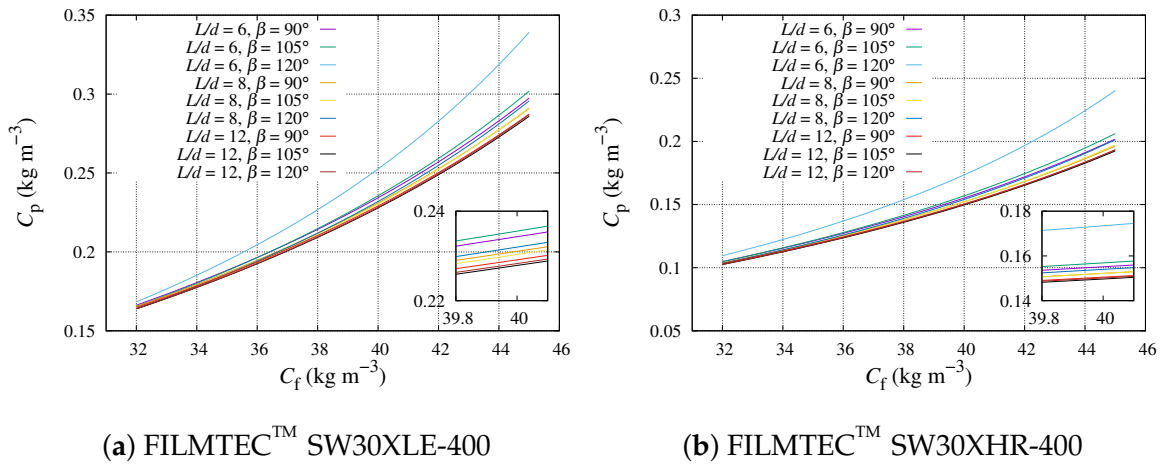


Figure 4. C_p of a PV with 8 SWMMs in series considering different feed spacer geometries, a range of C_f , $p_f = 55$ bar and $Q_f = 12 \text{ m}^3 \text{ h}^{-1}$.

Tables 4–6 show the results in terms of SEC, R and C_p in four different cases. Cases 1 and 2 with a standard C_f and Cases 3 and 4 with a high C_f . Table 4 shows the SEC for the two membranes studied in PVs of 6 and 8 SWMMs with different FSGs. The lowest SEC for both membranes and PVs were obtained for $L/d = 12$ and $\beta = 105^\circ$. As Q_f increased the differences between the aforementioned FSG and the rest in terms of SEC grew wider. The highest values of SEC were calculated for $L/d = 6$ and $\beta = 120^\circ$ in both membranes. The difference between maximum and minimum SEC was higher in PVs of 8 SWMMs in both membranes. The FSG had more impact on the SW30XHR-400, with greater differences between the maximum and minimum SEC values than with the SW30XLE-400.

Table 4. SEC (kWh m^{−3}) for PVs of 6 and 8 SWMMs with the two membranes studied with different FSGs.

Inputs	L/d	β	SW30XLE-400		SW30XHR-400	
			SEC(6/PV)	SEC(8/PV)	SEC(6/PV)	SEC(8/PV)
$C_f = 35$ $p_f = 55$ $Q_f = 8$ (Case 1)	6	90°	3.2914	3.0479	3.8109	3.3649
		105°	3.2792	3.0495	3.8013	3.3692
		120°	3.3023	3.1034	3.8536	3.4544
	8	90°	3.2710	3.0247	3.7821	3.3328
		105°	3.2475	3.0154	3.7578	3.3222
		120°	3.2497	3.0246	3.7635	3.3356
	12	90°	3.2576	3.0132	3.7651	3.3172
		105°	3.2454	3.0073	3.7499	3.3089
		120°	3.2461	3.0084	3.7515	3.3107
$C_f = 35$ $p_f = 55$ $Q_f = 12$ (Case 2)	6	90°	3.9377	3.4803	4.9215	4.1484
		105°	3.9527	3.5170	4.9680	4.2153
		120°	4.1757	3.8070	5.3489	4.6777
	8	90°	3.8828	3.4181	4.8392	4.0583
		105°	3.8692	3.4221	4.8420	4.0760
		120°	3.8945	3.4608	4.8925	4.1396
	12	90°	3.8492	3.3844	4.7914	4.0095
		105°	3.8267	3.3729	4.7710	3.9986
		120°	3.8347	3.3816	4.7840	4.0123
$C_f = 40$ $p_f = 60$ $Q_f = 8$ (Case 3)	6	90°	3.6702	3.4173	4.1936	3.7382
		105°	3.6550	3.4180	4.1796	3.7411
		120°	3.6759	3.4737	4.2255	3.8268
	8	90°	3.6486	3.3924	4.1639	3.7045
		105°	3.6216	3.3815	4.1347	3.6917
		120°	3.6232	3.3911	4.1388	3.7051
	12	90°	3.6342	3.3799	4.1455	3.6878
		105°	3.6201	3.3730	4.1280	3.6784
		120°	3.6208	3.3741	4.1296	3.6803
$C_f = 40$ $p_f = 60$ $Q_f = 12$ (Case 4)	6	90°	4.3298	3.8614	5.3280	4.5324
		105°	4.3398	3.8973	5.3678	4.5964
		120°	4.5577	4.1918	5.7365	5.0555
	8	90°	4.2738	3.7965	5.2460	4.4405
		105°	4.2550	3.7985	5.2416	4.4544
		120°	4.2773	3.8374	5.2874	4.5164
	12	90°	4.2386	3.7606	5.1964	4.3895
		105°	4.2120	3.7471	5.1703	4.3754
		120°	4.2200	3.7561	5.1836	4.3892

Table 5 shows the R for the two membranes studied in PVs of 6 and 8 SWMMs with different FSGs. The lowest R for both membranes and PVs were obtained for $L/d = 12$ and $\beta = 105^\circ$ as in the SEC. The results obtained for R had the same trend as SEC as both are closely related. Table 6 shows the C_p for the two membranes studied in PVs of 6 and 8 SWMMs with different FSGs. Considering the PVs of 6 SWMMs and Cases 1 and 3, the lowest C_p for the SW30XLE-400 were obtained for $L/d = 6$ and $\beta = 120^\circ$, and for the SW30XHR-400 for $L/d = 8$ and $\beta = 120^\circ$. When Q_f was increased, the minimum values of C_p were found in FSGs with $L/d = 12$ and $\beta = 105^\circ$ for both membranes and PVs. In Cases 1 and 3, the highest values of C_p were obtained for $L/d = 6$ and $\beta = 90^\circ$ in both membranes and PVs, while for Cases 2 and 4, the highest values of C_p were obtained for $L/d = 6$ and $\beta = 120^\circ$ in both membranes and PVs. The difference between the maximum and minimum value of C_p was higher as Q_f was increased for both membranes and PVs.

Table 5. R (%) for PVs of 6 and 8 SWMMs with the two membranes studied with different FSGs.

Inputs	L/d	β	SW30XLE-400		SW30XHR-400	
			$R(6/PV)$	$R(8/PV)$	$R(6/PV)$	$R(8/PV)$
$C_f = 35$ $p_f = 55$ $Q_f = 8$ (Case 1)	6	90°	46.42	50.13	40.09	45.40
		105°	46.59	50.10	40.19	45.35
		120°	46.26	49.23	39.65	44.23
	8	90°	46.71	50.51	40.40	45.84
		105°	47.04	50.67	40.66	45.99
		120°	47.01	50.51	40.59	45.80
	12	90°	46.90	50.70	40.58	46.06
		105°	47.08	50.80	40.74	46.17
		120°	47.06	50.78	40.72	46.15
$C_f = 35$ $p_f = 55$ $Q_f = 12$ (Case 2)	6	90°	38.80	43.90	31.04	36.83
		105°	38.65	43.44	30.75	36.24
		120°	36.59	40.13	28.56	32.66
	8	90°	39.35	44.70	31.57	37.65
		105°	39.49	44.64	31.55	37.48
		120°	39.23	44.15	31.23	36.91
	12	90°	39.69	45.14	31.89	38.10
		105°	39.92	45.30	32.02	38.21
		120°	39.84	45.18	31.94	38.08
$C_f = 40$ $p_f = 60$ $Q_f = 8$ (Case 3)	6	90°	45.41	48.77	39.74	44.59
		105°	45.60	48.76	39.88	44.55
		120°	45.34	47.98	39.44	43.55
	8	90°	45.68	49.13	40.03	44.99
		105°	46.02	49.29	40.31	45.15
		120°	46.00	49.15	40.27	44.98
	12	90°	45.86	49.31	40.20	45.19
		105°	46.04	49.41	40.37	45.31
		120°	46.03	49.40	40.36	45.29
$C_f = 40$ $p_f = 60$ $Q_f = 12$ (Case 4)	6	90°	38.49	43.16	31.28	36.77
		105°	38.40	42.77	31.05	36.26
		120°	36.57	39.76	29.05	32.97
	8	90°	39.00	43.90	31.77	37.53
		105°	39.17	43.88	31.80	37.42
		120°	38.97	43.43	31.52	36.90
	12	90°	39.32	44.32	32.07	37.97
		105°	39.57	44.48	32.24	38.09
		120°	39.49	44.37	32.15	37.97

Tables 7 and 8 show the results in terms of gradients of SEC and C_p in four different cases. The C_f in these four cases represent the minimum and maximum values of the most common seawater concentrations (32 g L^{-1} for Cases 5 and 6, and 37 g L^{-1} for Cases 7 and 8). Table 7 shows the SEC differences between PVs of 6–7 ($\Delta SEC(6-7)$) and 7–8 ($\Delta SEC(7-8)$) SWMMs of the SW30XLE-400 and SW30XHR-400 membranes, in different operating points. The highest differences were found in $\Delta SEC(6-7)$ for both membranes. In all cases, wider differences corresponded to $\beta = 90^\circ$. Depending on the operating point and the membrane, the highest differences were obtained for $L/d = 8$ and 12. For Case 5 (higher Q_f) the highest differences were obtained in $L/d = 8$ for the SW30XLE-400 and in $L/d = 12$ for the SW30XHR-400. This was due to different permeability coefficients and flow patterns (higher R for SW30XLE-400 implies lower Q_{fb} and Re). The higher the Re the higher the Δp_{fb} affecting R , SEC and C_p . This is the reason why differences in terms of ΔSEC were higher for the SW30XHR-400. Variations in $\Delta SEC(6-7)$ (considering the 4 cases) of between 20.2 and 27.3%

and of between 10.2 and 17.8% were obtained respectively for the SW30XLE-400 and SW30XHRE-400. $\Delta SEC(7 - 8)$ variations of between 23.2 and 38.2% and between 12.7 and 24.9% were calculated for the SW30XLE-400 and SW30XHRE-400, respectively. In terms of C_p , higher differences between PVs with 6 and 7 SWMMs and PVs with 7 and 8 elements were obtained for the SW30XHRE-400 than for the SW30XLE-400 (Table 8). This was due to the coefficient B of the SW30XHRE-400 membrane, which has a higher salt rejection. Consequently, C_m along the PV was higher (also affected by PF) for this membrane. Considering the 4 cases in terms of percentages, the variations of $\Delta C_p(7 - 6)$ and $\Delta C_p(8 - 7)$ were in a range of 4.6–17.5% and 6.3–30.9% for the SW30XLE-400 and in a range of 4.1–18.2% and 6.4–33.4% for the SW30XHRE-400. These percentages in terms of ΔSEC and ΔC_p show the impact of FSGs considering different operating points (Cases) in three types of PV (6, 7 and 8 SWMMs).

Table 6. C_p (mg L⁻¹) for PVs of 6 and 8 SWMMs with the two membranes studied with different FSGs.

Inputs	L/d	β	SW30XLE-400		SW30XHR-400	
			$C_p(6/PV)$	$C_p(8/PV)$	$C_p(6/PV)$	$C_p(8/PV)$
$C_f = 35$ $p_f = 55$ $Q_f = 8$ (Case 1)	6	90°	202.25	276.78	126.36	165.82
		105°	200.62	275.85	125.24	165.07
		120°	198.64	275.67	124.40	165.51
	8	90°	201.83	276.11	125.91	165.11
		105°	199.75	274.69	124.44	163.91
		120°	199.26	274.61	124.11	163.85
	12	90°	201.22	275.53	125.44	164.58
		105°	200.36	275.00	124.72	164.01
		120°	200.34	274.99	124.72	164.02
$C_f = 35$ $p_f = 55$ $Q_f = 12$ (Case 2)	6	90°	144.12	188.30	97.70	121.18
		105°	143.02	188.03	97.49	121.59
		120°	145.55	194.55	101.53	129.40
	8	90°	143.22	186.81	96.71	119.61
		105°	141.56	185.61	95.94	119.11
		120°	141.28	185.95	96.14	119.82
	12	90°	142.46	185.84	96.03	118.67
		105°	141.16	184.78	95.22	117.94
		120°	141.26	184.95	95.36	118.16
$C_f = 40$ $p_f = 60$ $Q_f = 8$ (Case 3)	6	90°	234.03	320.34	145.60	192.05
		105°	232.25	319.40	144.30	191.23
		120°	230.17	319.52	143.22	191.76
	8	90°	233.54	319.52	145.11	191.26
		105°	231.25	318.01	143.43	189.93
		120°	230.72	317.98	143.04	189.88
	12	90°	232.86	318.86	144.58	190.66
		105°	231.90	318.27	143.76	190.04
		120°	231.87	318.27	143.76	190.05
$C_f = 40$ $p_f = 60$ $Q_f = 12$ (Case 4)	6	90°	165.92	217.90	111.30	139.09
		105°	164.60	217.59	110.92	139.42
		120°	167.02	224.61	114.84	147.42
	8	90°	164.96	216.23	110.28	137.42
		105°	163.04	214.90	109.31	136.77
		120°	162.65	215.29	109.41	137.46
	12	90°	164.13	215.13	109.54	136.38
		105°	162.63	213.95	108.57	135.53
		120°	162.74	214.14	108.73	135.76

Table 7. ΔSEC (kWh m^{-3}) between PVs of 6 and 7 ($\Delta SEC(6-7)$), and 7 and 8 ($\Delta SEC(7-8)$) SWMMs for the two membranes studied with different FSGs.

Inputs	L/d	β	SW30XLE-400		SW30XHR-400	
			$\Delta SEC(6-7)$	$\Delta SEC(7-8)$	$\Delta SEC(6-7)$	$\Delta SEC(7-8)$
$C_f = 32$ $p_f = 50$ $Q_f = 8$ (Case 5)	6	90°	0.1567	0.1036	0.2784	0.1918
		105°	0.1491	0.0981	0.2711	0.1863
		120°	0.1316	0.0851	0.2540	0.1715
	8	90°	0.1582	0.1049	0.2800	0.1933
		105°	0.1507	0.0992	0.2733	0.1878
		120°	0.1467	0.0964	0.2693	0.1848
	12	90°	0.1573	0.1041	0.2794	0.1928
		105°	0.1537	0.1016	0.2760	0.1901
		120°	0.1536	0.1015	0.2759	0.1901
$C_f = 32$ $p_f = 50$ $Q_f = 12$ (Case 6)	6	90°	0.2830	0.1956	0.4612	0.3320
		105°	0.2718	0.1861	0.4504	0.3227
		120°	0.2330	0.1500	0.4015	0.2739
	8	90°	0.2868	0.1991	0.4660	0.3362
		105°	0.2782	0.1920	0.4581	0.3298
		120°	0.2711	0.1860	0.4511	0.3237
	12	90°	0.2873	0.1993	0.4666	0.3366
		105°	0.2819	0.1949	0.4618	0.3330
		120°	0.2815	0.1948	0.4612	0.3328
$C_f = 37$ $p_f = 55$ $Q_f = 8$ (Case 7)	6	90°	0.1617	0.1076	0.2857	0.1955
		105°	0.1527	0.1012	0.2770	0.1885
		120°	0.1322	0.0864	0.2559	0.1708
	8	90°	0.1637	0.1091	0.2879	0.1974
		105°	0.1548	0.1026	0.2798	0.1910
		120°	0.1501	0.0994	0.2747	0.1870
	12	90°	0.1628	0.1083	0.2872	0.1970
		105°	0.1586	0.1054	0.2829	0.1937
		120°	0.1583	0.1053	0.2829	0.1936
$C_f = 37$ $p_f = 55$ $Q_f = 12$ (Case 8)	6	90°	0.2916	0.1999	0.4786	0.3422
		105°	0.2778	0.1886	0.4650	0.3311
		120°	0.2334	0.1481	0.4118	0.2786
	8	90°	0.2964	0.2043	0.4838	0.3473
		105°	0.2859	0.1955	0.4745	0.3395
		120°	0.2769	0.1882	0.4659	0.3320
	12	90°	0.2971	0.2048	0.4849	0.3480
		105°	0.2902	0.1994	0.4788	0.3433
		120°	0.2896	0.1991	0.4784	0.3429

Table 8. ΔC_p (mg L⁻¹) between PVs of 7 and 6 ($\Delta C_p(7-6)$), and 8 and 7 ($\Delta C_p(8-7)$) SWMMs for the two membranes studied with different FSGs.

Inputs	<i>L/d</i>	β	SW30XLE-400		SW30XHR-400	
			$\Delta C_p(7-6)$	$\Delta C_p(8-7)$	$\Delta C_p(7-6)$	$\Delta C_p(8-7)$
$C_f = 32$ $p_f = 50$ $Q_f = 8$ (Case 5)	6	90°	32.44	33.86	17.04	17.86
		105°	32.77	34.19	17.21	18.05
		120°	33.74	35.12	17.90	18.80
	8	90°	32.29	33.73	16.89	17.72
		105°	32.56	34.03	16.98	17.84
		120°	32.78	34.22	17.12	17.98
	12	90°	32.27	33.74	16.83	17.67
		105°	32.42	33.88	16.88	17.74
		120°	32.43	33.89	16.89	17.75
$C_f = 32$ $p_f = 50$ $Q_f = 12$ (Case 6)	6	90°	19.28	20.11	10.52	10.74
		105°	19.71	20.59	10.88	11.13
		120°	22.07	23.21	13.11	13.65
	8	90°	18.93	19.76	10.18	10.39
		105°	19.13	20.00	10.33	10.56
		120°	19.47	20.36	10.62	10.87
	12	90°	18.78	19.63	10.02	10.24
		105°	18.86	19.74	10.05	10.28
		120°	18.90	19.78	10.10	10.32
$C_f = 37$ $p_f = 55$ $Q_f = 8$ (Case 7)	6	90°	38.36	39.81	20.45	21.40
		105°	38.79	40.21	20.67	21.64
		120°	40.00	41.35	21.51	22.56
	8	90°	38.16	39.63	20.27	21.22
		105°	38.52	39.99	20.40	21.38
		120°	38.79	40.23	20.58	21.57
	12	90°	38.14	39.63	20.21	21.17
		105°	38.32	39.80	20.29	21.25
		120°	38.34	39.81	20.29	21.26
$C_f = 37$ $p_f = 55$ $Q_f = 12$ (Case 8)	6	90°	23.09	24.06	12.59	12.90
		105°	23.61	24.64	13.00	13.34
		120°	26.28	27.59	15.39	16.05
	8	90°	22.68	23.63	12.22	12.51
		105°	22.94	23.96	12.39	12.71
		120°	23.35	24.39	12.72	13.06
	12	90°	22.49	23.47	12.04	12.34
		105°	22.62	23.63	12.08	12.40
		120°	22.67	23.67	12.13	12.45

4. Conclusions

The impact of different FSGs on SWRO membrane performance with different permeability coefficients was studied. It was observed that the longer the PV the higher the influence of the FSG on *SEC*. In terms of *SEC*, the membrane with a lower coefficient *A* suffered a more pronounced FSG impact. The effect of the FSG increased with Q_f . The impact of the FSG on C_p was slightly higher for the membrane with the lower coefficient *B* and increased with Q_f , with the differences between the maximum and minimum C_p values also increasing for both membranes. Manufacturers of RO SWMMs should take into consideration the installation of different FSGs in the same SWRO membranes. The option of having a membrane with different FSGs could help to improve SWRO plant operation. Normally, membrane manufacturers offer membranes with higher production or higher rejection (different permeability coefficients), different active area (400 or 440 ft²) or feed spacer

thickness (28 or 34 milli-inches. . .) but with a default FSG. It should be noted that this work is based on simulations and that the impact of membrane fouling can have different effects on different FSGs. This aspect was not considered in this study. The decrease of the coefficient A with fouling and operating time as well as due to CP were also not considered as it could be different for each FSG and different operating conditions. In term of costs, it should be considered that manufacturing SWMMs with different FSGs on request could increase the investment cost of the RO system. Operating and maintenance costs regarding the application of different FSGs in SWMMs would depend on the performance decay due to fouling, which depend not only on operating conditions but on the FSGs.

Author Contributions: Formal analysis, A.R.-G.; investigation, A.R.-G.; writing—original draft preparation, A.R.-G.; writing—review and editing, A.R.-G. and I.N.; supervision, I.N.; funding acquisition, A.R.-G. and I.N. All authors have read and agreed to the published version of the manuscript.

Funding: This research was funded by FEDER funds, EATIC RIS3 2014-2020 (project EATIC2017-010002).

Conflicts of Interest: The authors declare no conflict of interest.

Abbreviations

The following abbreviations are used in this manuscript:

Nomenclature

A	Water permeability coefficient ($\text{m d}^{-1} \text{ kg}^{-1} \text{ cm}^2$)
B	Ion permeability coefficient (m d^{-1})
C	Concentration (g l^{-1})
CFD	Computational fluid dynamics
CP	Concentration polarization
D	Diffusivity ($\text{m}^2 \text{ s}^{-1}$)
d	Filament diameter (m)
d_h	Hydraulic diameter (m)
FF	Flow factor
FSG	Feed spacer geometry
J	Flow per unit area ($\text{m}^3 \text{ m}^{-2} \text{ d}^{-1}$)
K_λ	Additional pressure losses factor
k	Mass transfer coefficient
L	Cylinder spacing (m)
m	Molal concentration (mol kg^{-1})
NDP	Net driven pressure (kg cm^{-2})
P	Solute pass (%)
PF	Polarization factor
PV	Pressure vessel
p	Pressure (kg cm^{-2})
Q	Flow ($\text{m}^3 \text{ d}^{-1}$)
R	Flow recovery (%)
Re	Reynolds number
RO	Reverse osmosis
S_m	Membrane surface (m^2)
Sc	Schmidt number
SEC	Specific energy consumption (kW h m^{-3})
Sh	Sherwood number
SWWM	Spiral wound membrane module
SWRO	Seawater reverse osmosis
T	Feed temperature ($^{\circ}\text{C}$)
TCF	Temperature correction factor
Y	Fraction recovery

Greek letters

β	Angle between crossing filaments
ε	Porosity of the cross-sectional area in the feed channel
η	Dynamic viscosity ($\text{kg m}^{-1} \text{s}$)
λ	Friction factor
ν	Velocity (m s^{-1})
π	Osmotic pressure (kg cm^{-2})
ρ	Density (kg m^{-3})
Δp	Pressure gradient (kg cm^{-2})
$\Delta \pi$	Osmotic pressure gradient (kg cm^{-2})
ΔC	Concentration gradient (mg l^{-1})

Subscripts

av	Average
f	Feed
fb	Feed-brine
m	Membrane
p	Permeate
b	Brine
s	Solute

References

- Qasim, M.; Badrelzaman, M.; Darwish, N.N.; Darwish, N.A.; Hilal, N. Reverse osmosis desalination: A state-of-the-art review. *Desalination* **2019**, *459*, 59–104. [\[CrossRef\]](#)
- Karabelas, A.J.; Koutsou, C.P.; Kostoglou, M.; Sioutopoulos, D.C. Analysis of specific energy consumption in reverse osmosis desalination processes. *Desalination* **2018**, *431*, 15–21. [\[CrossRef\]](#)
- Feo-García, J.; Ruiz-García, A.; Ruiz-Saavedra, E.; Melian-Martel, N. Energy consumption assessment of 4000 m^3/d SWRO desalination plants. *Desalin. Water Treat.* **2016**, *57*, 23019–23023. [\[CrossRef\]](#)
- Voutchkov, N. Energy use for membrane seawater desalination—Current status and trends. *Desalination* **2018**, *431*, 2–14. [\[CrossRef\]](#)
- Kurihara, M.; Takeuchi, H. SWRO-PRO System in “Mega-ton Water System” for Energy Reduction and Low Environmental Impact. *Water* **2018**, *10*, 48. [\[CrossRef\]](#)
- Park, H.G.; Kwon, Y.N. Long-Term Stability of Low-Pressure Reverse Osmosis (RO) Membrane Operation—A Pilot Scale Study. *Water* **2018**, *10*, 93. [\[CrossRef\]](#)
- Zhao, D.L.; Japip, S.; Zhang, Y.; Weber, M.; Maletzko, C.; Chung, T.S. Emerging thin-film nanocomposite (TFN) membranes for reverse osmosis: A review. *Water Res.* **2020**, *173*, 115557. [\[CrossRef\]](#)
- Saleem, H.; Zaidi, S.J. Nanoparticles in reverse osmosis membranes for desalination: A state of the art review. *Desalination* **2020**, *475*, 114171. [\[CrossRef\]](#)
- Okamoto, Y.; Lienhard, J.H. How RO membrane permeability and other performance factors affect process cost and energy use: A review. *Desalination* **2019**, *470*, 114064. [\[CrossRef\]](#)
- Chen, C.; Qin, H. A Mathematical Modeling of the Reverse Osmosis Concentration Process of a Glucose Solution. *Processes* **2019**, *7*, 271. [\[CrossRef\]](#)
- Anis, S.F.; Hashaikeh, R.; Hilal, N. Reverse osmosis pretreatment technologies and future trends: A comprehensive review. *Desalination* **2019**, *452*, 159–195. [\[CrossRef\]](#)
- Li, Y.; Yang, S.; Zhang, K.; Van der Bruggen, B. Thin film nanocomposite reverse osmosis membrane modified by two dimensional laminar MoS_2 with improved desalination performance and fouling-resistant characteristics. *Desalination* **2019**, *454*, 48–58. [\[CrossRef\]](#)
- Haidari, A.H.; Heijman, S.G.J.; van der Meer, W.G.J. Effect of spacer configuration on hydraulic conditions using PIV. *Sep. Purif. Technol.* **2018**, *199*, 9–19. [\[CrossRef\]](#)
- Ruiz-García, A.; de la Nuez Pestana, I. Feed Spacer Geometries and Permeability Coefficients. Effect on the Performance in BWRO Spiral-Wound Membrane Modules. *Water* **2019**, *11*, 152. [\[CrossRef\]](#)
- Abid, H.S.; Johnson, D.J.; Hashaikeh, R.; Hilal, N. A review of efforts to reduce membrane fouling by control of feed spacer characteristics. *Desalination* **2017**, *420*, 384–402. [\[CrossRef\]](#)

16. Haidari, A.H.; Heijman, S.G.J.; van der Meer, W.G.J. Optimal design of spacers in reverse osmosis. *Sep. Purif. Technol.* **2018**, *192*, 441–456. [\[CrossRef\]](#)
17. Xie, P.; Murdoch, L.C.; Ladner, D.A. Hydrodynamics of sinusoidal spacers for improved reverse osmosis performance. *J. Membr. Sci.* **2014**, *453*, 92–99. [\[CrossRef\]](#)
18. Schock, G.; Miquel, A. Mass transfer and pressure loss in spiral wound modules. *Desalination* **1987**, *64*, 339–352. [\[CrossRef\]](#)
19. Geraldès, V.; Pereira, N.E.; de Pinho, M.N. Simulation and Optimization of Medium-Sized Seawater Reverse Osmosis Processes with Spiral-Wound Modules. *Ind. Eng. Chem. Res.* **2005**, *44*, 1897–1905. [\[CrossRef\]](#)
20. Abbas, A. Simulation and analysis of an industrial water desalination plant. *Chem. Eng. Process.* **2005**, *44*, 999–1004. [\[CrossRef\]](#)
21. Costa, A.D.; Fane, A.; Wiley, D. Spacer characterization and pressure drop modelling in spacer-filled channels for ultrafiltration. *J. Membr. Sci.* **1994**, *87*, 79–98. [\[CrossRef\]](#)
22. Schwinge, J.; Neal, P.R.; Wiley, D.E.; Fletcher, D.F.; Fane, A.G. Spiral wound modules and spacers: Review and analysis. *J. Membr. Sci.* **2004**, *242*, 129–153. [\[CrossRef\]](#)
23. Koutsou, C.P.; Yiantsios, S.G.; Karabelas, A.J. Direct numerical simulation of flow in spacer-filled channels: Effect of spacer geometrical characteristics. *J. Membr. Sci.* **2007**, *291*, 53–69. [\[CrossRef\]](#)
24. Koutsou, C.P.; Yiantsios, S.G.; Karabelas, A.J. A numerical and experimental study of mass transfer in spacer-filled channels: Effects of spacer geometrical characteristics and Schmidt number. *J. Membr. Sci.* **2009**, *326*, 234–251. [\[CrossRef\]](#)
25. Liang, Y.Y.; Toh, K.Y.; Weihs, G.A.F. 3D CFD study of the effect of multi-layer spacers on membrane performance under steady flow. *J. Membr. Sci.* **2019**, *580*, 256–267. [\[CrossRef\]](#)
26. Toh, K.Y.; Liang, Y.Y.; Lau, W.J.; Weihs, G.A.F. 3D CFD study on hydrodynamics and mass transfer phenomena for SWM feed spacer with different floating characteristics. *Chem. Eng. Res. Des.* **2020**, *159*, 36–46. [\[CrossRef\]](#)
27. Kaviani-pour, O.; Ingram, G.D.; Vuthaluru, H.B. Studies into the mass transfer and energy consumption of commercial feed spacers for RO membrane modules using CFD: Effectiveness of performance measures. *Chem. Eng. Res. Des.* **2019**, *141*, 328–338. [\[CrossRef\]](#)
28. Wang, Y.; He, W.; Müller, J.D. Sensitivity analysis and gradient-based optimisation of feed spacer shape in reverse osmosis membrane processes using discrete adjoint approach. *Desalination* **2019**, *449*, 26–40. [\[CrossRef\]](#)
29. Guillen, G.; Hoek, E.M. Modeling the impacts of feed spacer geometry on reverse osmosis and nanofiltration processes. *Chem. Eng. J.* **2009**, *149*, 221–231. [\[CrossRef\]](#)
30. Haidari, A.H.; Heijman, S.G.J.; Uijttewaalt, W.S.J.; van der Meer, W.G.J. Determining effects of spacer orientations on channel hydraulic conditions using PIV. *J. Water Process Eng.* **2019**, *31*, 100820. [\[CrossRef\]](#)
31. Lu, Y.Y.; Hu, Y.D.; Zhang, X.L.; Wu, L.Y.; Liu, Q.Z. Optimum design of reverse osmosis system under different feed concentration and product specification. *J. Membr. Sci.* **2007**, *287*, 219–229. [\[CrossRef\]](#)
32. Vince, F.; Marechal, F.; Aoustin, E.; Bréant, P. Multi-objective optimization of RO desalination plants. *Desalination* **2008**, *222*, 96–118. [\[CrossRef\]](#)
33. Sassi, K.M.; Mujtaba, I.M. Optimal design and operation of reverse osmosis desalination process with membrane fouling. *Chem. Eng. J.* **2011**, *171*, 582–593. [\[CrossRef\]](#)
34. Du, Y.; Xie, L.; Wang, Y.; Xu, Y.; Wang, S. Optimization of Reverse Osmosis Networks with Spiral-Wound Modules. *Ind. Eng. Chem. Res.* **2012**, *51*, 11764–11777. [\[CrossRef\]](#)
35. Altaee, A. Computational model for estimating reverse osmosis system design and performance: Part-one binary feed solution. *Desalination* **2012**, *291*, 101–105. [\[CrossRef\]](#)
36. Saavedra, E.R.; Gotor, A.G.; Báez, S.O.P.; Martín, A.R.; Ruiz-García, A.; González, A.C. A design method of the RO system in reverse osmosis brackish water desalination plants (procedure). *Desalin. Water Treat.* **2013**, *51*, 4790–4799. [\[CrossRef\]](#)
37. Ruiz-Saavedra, E.; Ruiz-García, A.; Ramos-Martín, A. A design method of the RO system in reverse osmosis brackish water desalination plants (calculations and simulations). *Desalin. Water Treat.* **2015**, *55*, 2562–2572. [\[CrossRef\]](#)
38. Choi, J.S.; Kim, J.T. Modeling of full-scale reverse osmosis desalination system: Influence of operational parameters. *J. Ind. Eng. Chem.* **2015**, *21*, 261–268. [\[CrossRef\]](#)

39. Avlonitis, S.A.; Pappas, M.; Moutesidis, K. A unified model for the detailed investigation of membrane modules and RO plants performance. *Desalination* **2007**, *203*, 218–228. [[CrossRef](#)]
40. Ruiz-García, A.; de la Nuez-Pestana, I. A computational tool for designing BWRO systems with spiral wound modules. *Desalination* **2018**, *426*, 69–77. [[CrossRef](#)]
41. Wijmans, J.G.; Baker, R.W. The solution-diffusion model: A review. *J. Membr. Sci.* **1995**, *107*, 1–21. [[CrossRef](#)]
42. Al-Obaidi, M.A.; Kara-Zaitri, C.; Mujtaba, I.M. Scope and limitations of the irreversible thermodynamics and the solution diffusion models for the separation of binary and multi-component systems in reverse osmosis process. *Comput. Chem. Eng.* **2017**, *100*, 48–79. [[CrossRef](#)]
43. Hinkle, K.R.; Wang, X.; Gu, X.; Jameson, C.J.; Murad, S. Computational Molecular Modeling of Transport Processes in Nanoporous Membranes. *Processes* **2018**, *6*, 124. [[CrossRef](#)]
44. Kucera, J. *Reverse Osmosis: Industrial Processes and Applications*; John Wiley & Sons: Hoboken, NJ, USA, 2015.
45. Ruiz-García, A.; Nuez, I. Long-term performance decline in a brackish water reverse osmosis desalination plant. Predictive model for the water permeability coefficient. *Desalination* **2016**, *397*, 101–107. [[CrossRef](#)]
46. Ruiz-García, A.; Melián-Martel, N.; Nuez, I. Short Review on Predicting Fouling in RO Desalination. *Membranes* **2017**, *7*. [[CrossRef](#)]
47. Du, Y.; Xie, L.; Liu, J.; Wang, Y.; Xu, Y.; Wang, S. Multi-objective optimization of reverse osmosis networks by lexicographic optimization and augmented epsilon constraint method. *Desalination* **2014**, *333*, 66–81. [[CrossRef](#)]
48. Water, D.; Solutions, P. *Filmtec Reverse Osmosis Membranes Technical Manual*; Dow Water and Process Solutions: Midland, MI, USA, 2005.
49. Mulder, M. *Basic Principles of Membrane Technology*; Springer Science & Business Media: Berlin/Heidelberg, Germany, 2012.
50. Boudinar, M.; Hanbury, W.; Avlonitis, S. Numerical simulation and optimisation of spiral-wound modules. *Desalination* **1992**, *86*, 273–290. [[CrossRef](#)]



© 2020 by the authors. Licensee MDPI, Basel, Switzerland. This article is an open access article distributed under the terms and conditions of the Creative Commons Attribution (CC BY) license (<http://creativecommons.org/licenses/by/4.0/>).